Article

Novel Organic Sensitizers Containing 2,6-Difunctionalized Anthracene Unit for Dye Sensitized Solar Cells

Yung-Sheng Yen, Yung-Chung Chen, Hsien-Hsin Chou, Shih-Tang Huang and Jiann T. Lin *

Institute of Chemistry, Academia Sinica, Nankang, Taipei 11529, Taiwan;
E-Mails: ysyen@chem.sinica.edu.tw (Y.S.Y.); chenyc0701@chem.sinica.edu.tw (Y.C.C.);
hhchou@chem.sinica.edu.tw (H.H.C.); hstang0724@yahoo.com.tw (S.T.H.)

* Author to whom correspondence should be addressed; E-Mail: jtlin@gate.sinica.edu.tw;
Tel.: +886-2-27898522; Fax: +886-2-27831237.

Abstract: A series of new organic dyes comprising different amines as electron donors, 2-(6-substituted-anthracen-2-yl)-thiophene as the π-conjugated bridge, and cyanoacrylic acid group as an electron acceptor and anchoring group, have been synthesized. There exists charge transfer transition from arylamine and anthracene to the acceptor in these compounds, as evidenced from the photophysical measurements and the computational results. Under one sun (AM 1.5) illumination, dye-sensitized solar cells (DSSCs) using these dyes as the sensitizers exhibited efficiencies ranging from 1.62% to 2.88%, surpassing that using 9,10-difunctionalized anthracene-based sensitizer.

1. Introduction

Dye-sensitized solar cells (DSSCs) have been investigated extensively as promising candidates for renewable-energy sources since the first report by O'Regan and Grätzel in 1991 [1]. As a critical component in DSSCs, the sensitizer plays a vital role in the light harvesting efficiency providing electron injection into the conduction band of an oxide semiconductor (e.g., TiO_2) upon light excitation. DSSCs based on Ru complex dyes have achieved a high photoelectric conversion yield (η) of almost 12.0% under standard AM 1.5 sunlight irradiation [2–4]. Recently, conversion yield exceeding 12.0% has also been demonstrated for DSSCs based on zinc porphyrin dye [5]. Compared

with Ru complexes, environmental friendly metal-free organic dyes are considered to be an alternative due to their high molar absorption coefficient, low cost, and easy molecular tailoring and synthesis [6–12]. Organic sensitizers used for efficient DSSC devices are generally composed of three units: including a donor, an acceptor (also as the anchor to the nanocrystalline TiO_2 surface), and a π-conjugated spacer connecting the donor and the spacer. An ideal spacer should allow effective photoinduced intramolecular charge transfer from the donor to the acceptor. Meanwhile, intermolecular dye aggregation and recombination of conduction-band electrons with triiodide present in the electrolyte have to be suppressed. In recent years, we have been interested in push–pull type metal-free sensitizers using arylamine as the electron donor and 2-cyanoacrylic acid as the electron acceptor [13–21]. In continuation of our studies on sensitizers, we became interested in dyes containing fused aromatic segments in the spacer based on the following reasons: (1) the rigid segment has less reorganization energy and may facilitate electron transfer; (2) rigid segments with a planar skeleton may reduce steric congestion and allow more compact dye packing on the TiO_2 surface.

Among rigid fused aromatic entities, anthracene has been widely used in opto-electronic materials such as organic thin film transistors [22–24], organic light-emiting diodes [25–30] and bulk heterojunction solar cells [31]. Recently, a few anthracene-based derivatives have been reported as sensitizers for DSSCs [32–34]. However, all previous reports have focused on anthracene derivatives substituted on C9 and C10. An alkynyl or alkenyl substituent has to be introduced at C9 and/or C10 in order to avoid serious steric congestion of the anthracene moiety with its neighboring aromatic rings, which results in a drop of the cell efficiency [32–34]. Recently, we reported new organic dyes containing a 1,4-naphthyl entity in the conjugation bridge [35]. We also found that the steric congestion between the naphthyl and aromatic moieties jeopardized charge transfer from the donor to the acceptor, consequently the best performance of the device reached only 62% of N719-based DSSC (7.31%). To further explore the possibility of using rigid aromatic segment for dye molecule, we decided to develop sensitizers incorporating 2,6-difuntionalized anthracene in the spacer, as the steric congestion will be largely alleviated compared to 9,10-disubstituted anthracenyl or 1,4-naphthyl derivatives. To the best of our knowledge, 2,6-difuntionalized anthracene-based sensitizers have never been explored for applications in DSSCs. In this paper, we report the synthesis and characterization of four organic dyes with conjugated subsituents at C2 and C6 positions of the anthracene core. To decrease dye aggregation and improve the solubility of the dyes, two long hydrophobic alkoxy chains were introduced at C9 and C10 positions of the anthracene. The photophysical properties of the compounds and the performance of the DSSCs fabricated from these dyes are also discussed.

2. Experimental Section

2.1. General Information

Unless otherwise specified, all the reactions were performed under nitrogen atmosphere using standard Schlenk techniques. All solvents used were purified by standard procedures, or purged with nitrogen before use. ^{1}H NMR spectra were recorded on a Bruker 300-MHz or 400-MHz spectrometer. Absorption spectra were recorded on a Cary 50 probe UV-Vis spectrophotometer. All chromatographic separations were carried out on silica gel (60 M, 230–400 mesh). Mass spectra (FAB) were recorded

on a VG70-250S mass spectrometer. The photoelectrochemical characterizations on the solar cells were carried out using an Oriel Class A solar simulator (Oriel 91195A, Newport Corp.). Photocurrent-voltage characteristics of the DSSCs were recorded with a potentiostat/galvanostat (CHI650B, CH Instruments, Inc.) at a light intensity of 100 mW cm^{-2} calibrated by an Oriel reference solar cell (Oriel 91150, Newport Corp.). The monochromatic quantum efficiency was recorded through a monochromator (Oriel 74100, Newport Corp.) at short circuit condition. The intensity of each wavelength was in the range of 1–3 mW cm^{-2}. Electrochemical impedance spectra (EIS) were recorded for DSSC under illumination at open-circuit voltage (V_{OC}) or dark at −0.55 V potential at room temperature. The frequencies explored ranged from 10 mHz to 100 kHz. The TiO$_2$ nanoparticles and the reference compound, **N719**, were purchased from Solaronix, S.A., Switzerland.

2.2. Synthesis

All the new dyes were prepared via Knoevenagel condensation reaction by reacted corresponding aldehyde derivatives and cyanoacetic acid in the presence catalytic amount of ammonium acetate.

*2-Cyano-3-(5-(6-(diphenylamino)-9,10-bis(hexyloxy)anthracen-2-yl)thiophen-2-yl)acrylic acid (**An-1**).* Spectroscopic data for **An-1**: ^{1}H NMR (400 MHz, acetone-d_6): δ 8.63 (d, *J* = 1.6 Hz, 1H), 8.46 (s, 1H), 8.24 (d, *J* = 8.8 Hz, 1H), 8.22 (d, *J* = 8.8 Hz, 1H), 8.04 (d, *J* = 4.0 Hz, 1H), 7.68–7.84 (m, 4H), 7.32 (dd, *J* = 8.8, 2.4 Hz, 1H), 7.79 (d, *J* = 8.0 Hz, 2H), 7.53 (d, *J* = 4.0 Hz, 1H), 7.41–7.27 (m, 10H), 7.24–7.16 (m, 6H), 4.25 (t, *J* = 6.4 Hz, 2H), 3.95 (t, *J* = 6.4 Hz, 2H), 1.85–1.64 (m, 4H), 1.46–1.40 (m, 6H), 0.95–0.90 (m, 6H). ^{13}C NMR (CDCl$_3$): δ 168.1, 156.5, 148.8, 147.5, 147.2, 145.8, 139.9, 134.5, 129.4, 128.3, 125.2, 124.6, 123.4, 123.8, 123.5, 123.1, 122.8, 121.0, 115.5, 96.2, 75.6, 31.8, 30.6, 30.3, 26.0, 25.6, 22.7, 22.5, 14.1. MS (FAB): *m/z* 722.1 (calcd [M]$^+$). HRMS m/z [M + H]$^+$ calculated for C$_{46}$H$_{46}$N$_2$O$_4$S, 723.3256 found: 723.3282.

*3-(5-(9,10-Bis(hexyloxy)-6-(naphthalen-1-yl(phenyl)amino)anthracen-2-yl)thiophen-2-yl)-2-cyanoacrylic acid (**An-2**).* Spectroscopic data for **An-2**: ^{1}H NMR (400 MHz, acetone-d_6): δ 8.61 (d, *J* = 1.2 Hz, 1H), 8.45 (s, 1H), 8.21 (d, *J* = 8.0 Hz, 1H), 8.18 (d, *J* = 8.0 Hz, 1H), 8.05–8.00 (m, 3H), 7.97 (d, *J* = 8.0 Hz, 1H), 7.84–7.82 (m, 2H), 7.63 (t, *J* = 7.2 Hz, 1H), 7.53 (t, *J* = 7.2 Hz, 1H), 7.46 (d, *J* = 8.0 Hz, 1H), 7.43–7.34 (m, 5H), 7.25 (d, *J* = 8.0 Hz, 2H), 7.13 (t, *J* = 7.2 Hz, 1H), 4.24 (t, *J* = 6.8 Hz, 2H), 3.90 (t, *J* = 6.8 Hz, 2H), 1.81–1.71 (m, 4H), 1.49–1.21 (m, 6H), 0.92 (t, *J* = 7.8 Hz, 6H). ^{13}C NMR (CDCl$_3$): δ 168.2, 156.5, 148.8, 147.5, 147.4, 146.2, 145.7, 143.1, 139.9, 135.2, 134.4, 130.9, 129.2, 128.4, 127.8, 127.3, 127.1, 126.8, 126.4, 126.3, 126.1, 125.1, 124.5, 124.0, 123.9, 123.6, 123.4, 123.2, 123.1, 122.7, 122.5, 121.0, 115.5, 109.5, 96.1, 75.7, 31.7, 31.6, 30.6, 30.1, 26.0, 25.4, 22.6, 22.5, 14.1, 14.0. MS (FAB): *m/z* 772.1 (calcd [M]$^+$). HRMS m/z [M]$^+$ calculated for C$_{50}$H$_{48}$N$_2$O$_4$S, 772.3177 found: 772.3193.

*3-(5-(6-(Bis(9,9-diethyl-9H-fluoren-2-yl)amino)-9,10-bis(hexyloxy)anthracen-2-yl)thiophen-2-yl)-2-cyanoacrylic acid (**An-3**).* Spectroscopic data for **An-3**: ^{1}H NMR (400 MHz, acetone-d_6): δ δ 8.54 (d, *J* = 1.2 Hz, 1H), 8.45 (s, 1H), 8.25 (d, *J* = 8.4 Hz, 1H), 8.02 (d, *J* = 4.0 Hz, 1H), 7.98–7.78 (m, 7H), 7.73 (d, *J* = 2.0 Hz, 1H), 7.46 (dd, *J* = 8.4, 2.4 Hz, 1H), 7.41 (d, *J* = 7.2 Hz, 2H), 7.37–7.30 (m, 9H), 4.28 (t, *J* = 6.4 Hz, 2H), 3.95 (t, *J* = 6.8 Hz, 2H), 1.90–1.63 (m, 8H), 1.59–1.11 (m, 10H), 0.94 (t, *J* = 6.4 Hz, 3H), 0.74 (t, *J* = 6.4 Hz, 3H), 0.37 (t, *J* = 7.2 Hz, 12 H). ^{13}C NMR (CDCl$_3$): δ 167.7, 156.6, 149.8, 148.8, 147.6, 146.7, 146.1, 141.2, 139.8, 137.5, 134.5, 128.1, 126.9, 126.5, 124.7, 124.4, 123.9,

123.0, 122.8, 121.2, 120.8, 120.3, 119.7, 119.2, 115.6, 96.4, 56.2, 32.7, 31.8, 31.6, 30.6, 30.3, 26.0, 25.7, 22.6, 22.4, 14.1, 13.9, 8.6. MS (FAB): *m/z* 1011.3 (calcd [M]$^+$). HRMS m/z [M + H]$^+$ calculated for $C_{68}H_{70}N_2O_4S$, 1011.5134 found: 1011.5176.

3-(5-(6-(Anthracen-2-yl(phenyl)amino)-9,10-bis(hexyloxy)anthracen-2-yl)thiophen-2-yl)-2-cyanoacrylic acid (An-4). Spectroscopic data for **An-4**: ^{1}H NMR (400 MHz, acetone-d_6): δ δ 8.65 (d, *J* = 1.6 Hz, 1H), 8.52 (s, 1H), 8.45 (s, 1H), 8.34 (s, 1H), 8.27 (d, *J* = 7.2 Hz, 1H), 8.25 (d, *J* = 7.2 Hz, 1H), 8.09 (d, *J* = 8.0 Hz, 1H), 8.06 (dd, *J* = 8.0, 4.0 Hz, 1H), 8.02 (d, J = 4.0 Hz, 1H), 7.97 (dd, *J* = 8.0, 4.0 Hz, 1H), 7.88 (dd, 8.0, 1.6 Hz, 1H), 7.85 (d, *J* = 4.0 Hz, 1H), 7.75 (d, *J* = 2.4 Hz, 1H), 7.72 (d, *J* = 1.2 Hz, 1H), 7.48–7.41 (m, 6H), 7.34 (d, *J* = 8.0 Hz, 2H), 7.25 (t, *J* = 7.2 Hz, 1H), 4.28 (t, *J* = 6.8 Hz, 2H), 3.96 (t, *J* = 6.8 Hz, 2H), 1.90–1.63 (m, 4H), 1.55–1.48 (m, 6H), 0.97–0.92 m, 6H). ^{13}C NMR (CDCl$_3$): δ 167.2, 156.3, 148.9, 147.4, 147.0, 146.1, 145.5, 144.2, 139.7, 134.6, 132.5, 132.2, 131.2, 129.5, 129.3, 128.1, 127.8, 127.3, 126.0, 125.6, 125.2, 125.1, 124.9, 124.8, 124.6, 124.5, 124.2, 124.1, 123.8, 123.3, 123.1, 121.1, 120.1, 115.7, 112.9, 96.5, 76.2, 67.9, 31.8, 31.6, 30.6, 30.3, 26.0, 25.6, 22.6, 22.3, 14.1, 13.9. MS (FAB): *m/z* 823.3 (calcd [M]$^+$). HRMS m/z [M]$^+$ calculated for $C_{54}H_{50}N_2O_4S$, 822.3491 found: 822.3511.

2.3. Devices Fabrication

The photoanode used was the TiO$_2$ thin film (12 μm of 20 nm particles as the absorbing layer and 6 μm of 400 nm particles as the scattering layer) coated on FTO glass substrate with a dimension of 0.5×0.5 cm^2 [35]. The film thickness measured by a profilometer (Dektak3, Veeco/Sloan Instruments Inc., USA). A platinized FTO produced by thermopyrolysis of H$_2$PtCl$_6$ was used as a counter electrode. The TiO$_2$ thin film was dipped into the THF solution containing 3×10^{-4} M dye sensitizers for at least 12 h. After rinsing with THF, the photoanode adhered with a polyester tape of 60 μm in thickness and with a square aperture of 0.36 cm^2 was placed on top of the counter electrode and tightly clipping them together to form a cell. Electrolyte was then injected into the space and then sealing the cell with the Torr Seal cement (Varian, MA, USA). The electrolyte was composed of 0.5 M lithium iodide (LiI), 0.05 M iodine (I$_2$), and 0.5 M 4-*tert*-butylpyridine that was dissolved in acetonitrile.

2.4. Quantum Chemistry Computation

The computations were performed with Q-Chem 4.0 software [36]. Geometry optimization of the molecules were performed using hybrid B3LYP functional and 6-31G* basis set. For each molecule, a number of possible conformations were examined and the one with the lowest energy was used. The same functional was also applied for the calculation of excited states using time-dependent density functional theory (TD–DFT). There exist a number of previous works that employed TD–DFT to characterize excited states with charge-transfer character [37,38]. In some cases underestimation of the excitation energies was seen [36,39]. Therefore, in the present work, we use TD–DFT to visualize the extent of transition moments as well as their charge-transfer characters, and avoid drawing conclusions from the excitation energy.

3. Results and Discussion

3.1. Synthesis

Scheme 1 illustrates the synthetic route towards the target molecules (**An-1** to **An-4**). Kumada cross-coupling [40] of thienyl magnesium bromide with 2,6-dibromo-9,10-dihexyloxyanthracene (**1**) generated **2** with a monosubstituent, which then underwent C–N coupling reaction [41,42] with diarylamine to afford **3a–3d**. These intermediates were conveniently converted to aldehydes (**4a–4d**) by lithiation with *n*-butyllithium followed by quenching with dimethylformamide. The aldehydes were converted to the dyes via Knoevenagel condensation with cyanoacetic acid in acetic acid in the presence of ammonium acetate as the catalyst. The final target dyes are obtained as dark red powders, and are soluble in common organic solvents such as THF, CH_2Cl_2, and $CHCl_3$.

Scheme 1. Synthesis of dyes **An-1** to **An-4**.

3a: Ar1 = Ar2 = phenyl
3b: Ar1 = phenyl; Ar2 = 1-naphthyl
3c: Ar1 = Ar2 = 9,9-diethyl-fluoren-2-yl
3d: Ar1 = phenyl; Ar2 = 2-anthracenyl

An-1: Ar1 = Ar2 = phenyl
An-2: Ar1 = phenyl; Ar2 = 1-naphthyl
An-3: Ar1 = Ar2 = 9,9-diethyl-fluoren-2-yl
An-4: Ar1 = phenyl; Ar2 = 2-anthracenyl

4a: Ar1 = Ar2 = phenyl
4b: Ar1 = phenyl; Ar2 = 1-naphthyl
4c: Ar1 = Ar2 = 9,9-diethyl-fluoren-2-yl
4d: Ar1 = phenyl; Ar2 = 2-anthracenyl
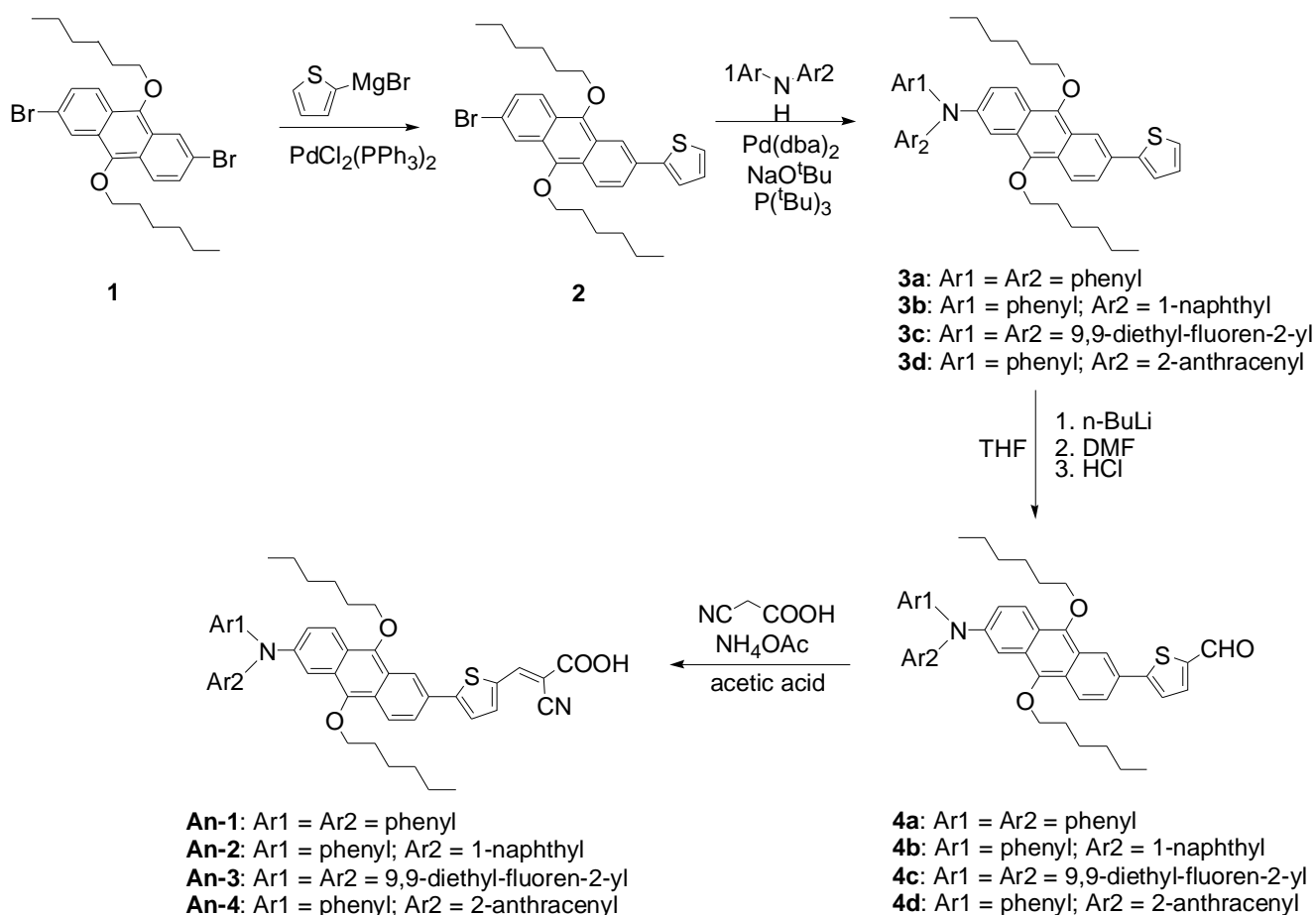
3.2. Optical Properties

The UV-Vis absorption spectra of the sensitizers **An-1** to **An-4** are shown in Figure 1, and their photophysical data are listed in Table 1. All dyes exhibit absorption bands in two distinct regions. The band(s) at 300–400 nm may be attributed to the π–π* electron transition of the conjugation backbone, and the band at around 450–550 nm has prominent intramolecular charge transfer (ICT) from the diarylamine and anthracene to 2-cyanoacrylic acid. The absorption band below 400 nm exhibited

vibronic characteristics of anthracenyl entity for all dyes except **An-3**. The vibronic pattern may be buried under the intense absorption band due to bis(fluorenyl)amino moiety [18]. The λ_{max} value of the ICT band decreases in the order of **An-3** > **An-4** > **An-1** ≈ **An-2**. The influence of the donor on the ICT band is evident: **An-3** has the longest absorption wavelength with the strongest absorption because of strong electron-donating ability of bis-diethylfluorenyl amino group [43]. The significantly bathochromic and hyperchromic shifts of the ICT band in **An-4** compared to **An-1** and **An-2** may also be attributed to the incorporation of electron excessive anthracenyl entity at the arylamino donor. Compound **An-1** exhibits absorption peak at 479 nm ($\varepsilon = 3.7 \times 10^4$ M^{-1}cm^{-1}), which is almost the same as that of **An-2** (477 nm, 3.48×10^4 M^{-1}cm^{-1}), indicating that the phenyl and naphthyl rings at the N atom have similar influence on the arylamine donor. It is interesting to compare the UV absorption for the 2,6-difuntionalized anthracene entity as the spacer between the donor and the acceptor is advantageous for intramolecular charge transfer compared to the 9,10-difuntionalized anthracene spacer, as witnessed from comparison of the spectra between **An-2** and a 9,10-difuntionalized anthracene-based dye (**5** in Figure 2) with a similar structure [34]. Compound **An-2** has red-shifted absorption with a higher molar extinction coefficients compared to **5** (434 nm, $\varepsilon = 1.31 \times 10^4$ M^{-1}cm^{-1}). Non-coplanar conformation of 9,10-difuntionalized anthracene undoubtedly jeopardizes the charge transfer.

Significant blue shift of the spectra of the dyes on TiO$_2$ surface (Figure 3) may be ascribed to the deprotonation of the carboxylic acid [16], which was also confirmed by measuring the absorption of the dyes in the presence of Et$_3$N. Certain degree of J-aggregation [44–46] may also occur, as evidenced from the prominent red tailing of the absorption spectra.

Figure 1. Absorption spectra of the dyes in THF solutions.
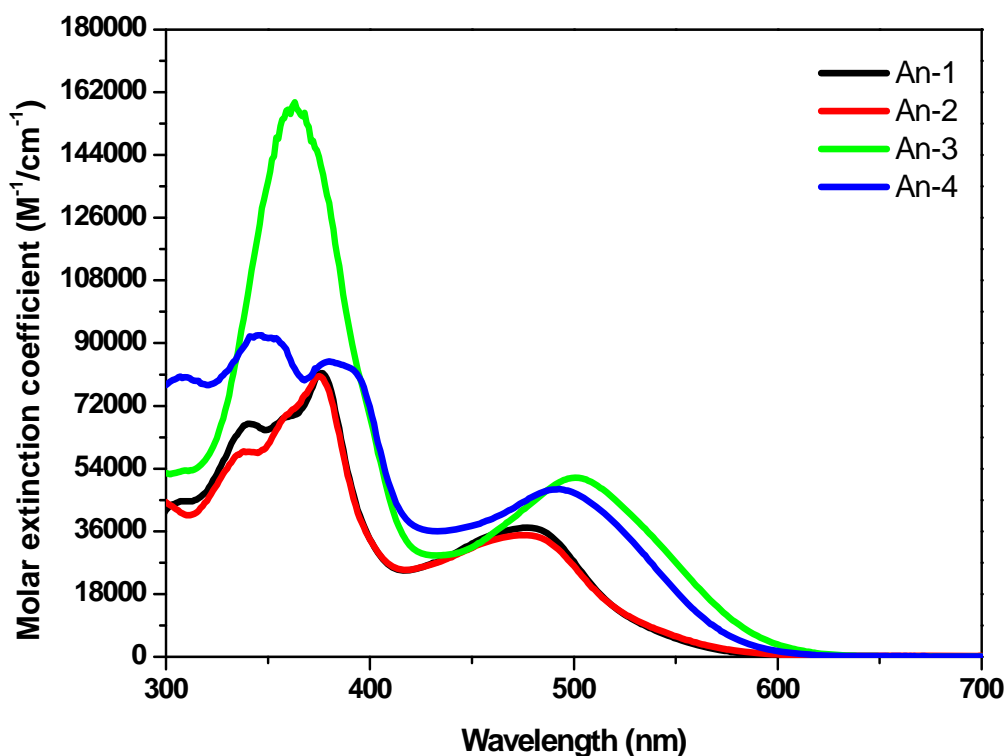
Table 1. Electrooptical and electrochemical parameters of the dyes.

Dye	λ_{abs} ($\varepsilon \times 10^{-4}$ M^{-1} cm^{-1})^a nm	$E_{1/2}$ (ox)^b mV	$E_{ox}{}^c$ V	$E_{0-0}{}^d$ eV	$E_{0-0}{}^{*e}$ V
An-1	479 (3.70), 376 (8.14)	348	1.05	2.29	−1.24
An-2	477 (3.48), 375 (8.05)	360	1.06	2.29	−1.23
An-3	500 (5.13), 363 (15.91)	312	1.01	2.12	−1.11
An-4	493 (4.81), 379 (8.47)	356	1.06	2.14	−1.08

^{a} Recorded in THF solutions at 298K. ^{b} Recorded in THF solutions. Oxidation potential reported is adjusted to the potential of ferrocene ($E_{1/2}$ (ox) = 212 mV *vs.* Ag/AgNO$_3$) which was used as an internal reference. Scan rate: 100 mV/s. ^{c} E_{ox}: The ground state oxidation potential *vs.* NHE. ^{d} The bandgap, E_{0-0}, was derived from the observed optical edge. ^{e} E_{0-0}*: The excited state oxidation potential *vs.* NHE.

Figure 2. Structure of the compound **5**.

5
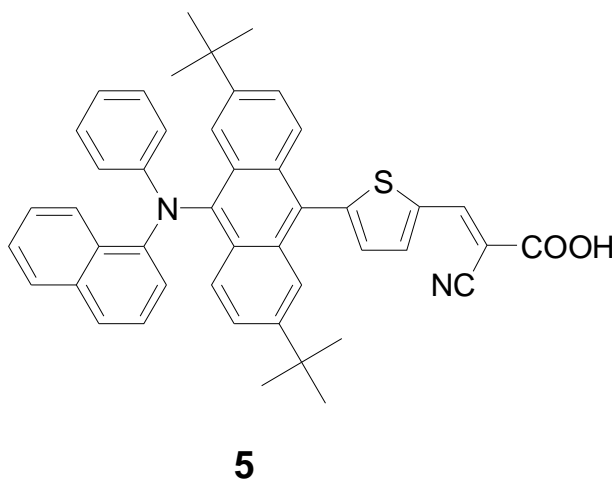
Figure 3. Absorption spectra of the dyes on TiO$_2$ films.
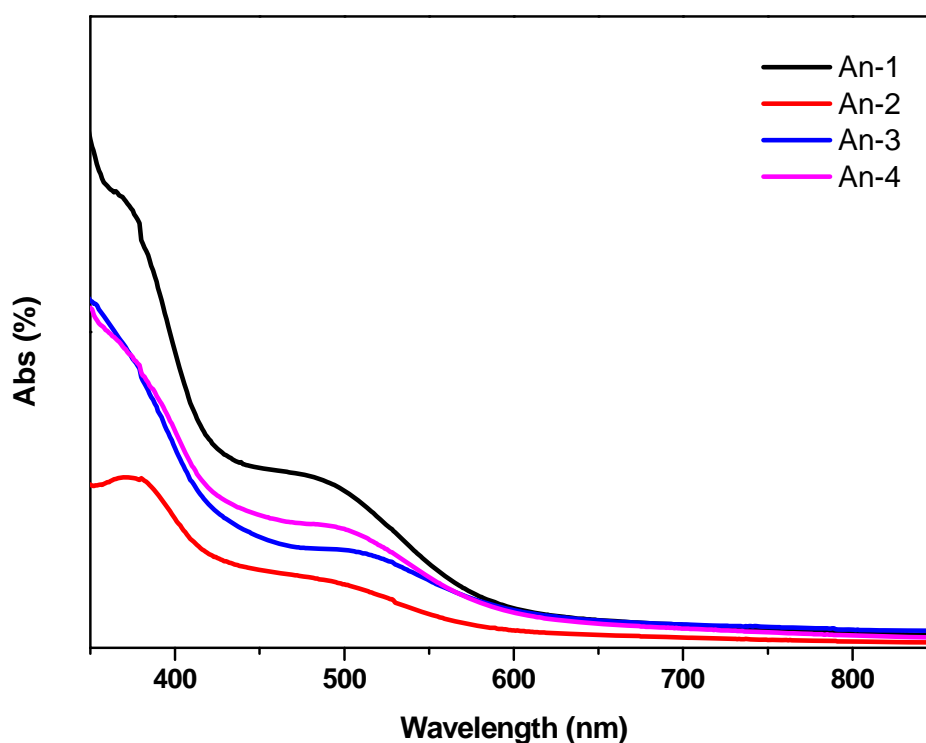
3.3. Optical Properties

The energetic alignment of highest occupied molecular orbital (HOMO) and lowest unoccupied molecular orbital (LUMO) energy levels is crucial for an efficient operation of the sensitizer in DSSCs. To judge the feasibility of electron transfer from the excited dye molecule to the conduction band of TiO_2 electrode, redox potentials of these dyes were investigated by cyclic voltammetry and the data are listed in Table 1. Representative cyclic voltammograms are shown in Figure 4. The redox potentials of these new dyes were measured in THF with 0.1 M tetra-butylammonium hexafluorophosphate. All the dyes exhibited one quasi-reversible redox wave due to the oxidation of arylamine. The oxidation potentials of **An-1**, **An-2**, **An-3** and **An-4** were measured to be 1.05, 1.06, 1.01 and 1.06 V versus NHE, respectively. The lowest oxidation potential of **An-3** is consistent with the presence of strong electron-donating bis-diethylfluorenyl amino group. All the oxidation potential are more positive than that of I^-/I_3^- (0.4 V *vs.* NHE) [47], ensuring favorable regeneration of dyes. The oxidation potentials of these materials were calculated with the energy gap (E_{0-0}, 2.12–2.29 eV) obtained from the cutoff wavelength of the absorption spectra was utilized to derive the excited state potentials. The excited state potential (*vs.* NHE) for sensitizers **An-1**, **An-2**, **An-3**, and **An-4** were calculated to be −1.24, −1.23, −1.11 and −1.08 V, respectively, indicating enough driving force for electron injection from the photo-excited sensitizers to the conduction band of the TiO_2 electrode (−0.5 V *vs.* NHE) [44]. These results clearly demonstrate that the novel dyes are potentially efficient dyes for DSSCs.

Figure 4. Cyclic voltammograms of **An-3** and **An-4** in deoxygenated THF containing 0.1 M TBAPF$_6$ at 25 °C. Ferrocene (Fc) was added as an internal standard. All potentials are in volts *vs.* Ag/AgNO$_3$ (0.01 M in MeCN; the scan rate is 100 mV s^{-1}).
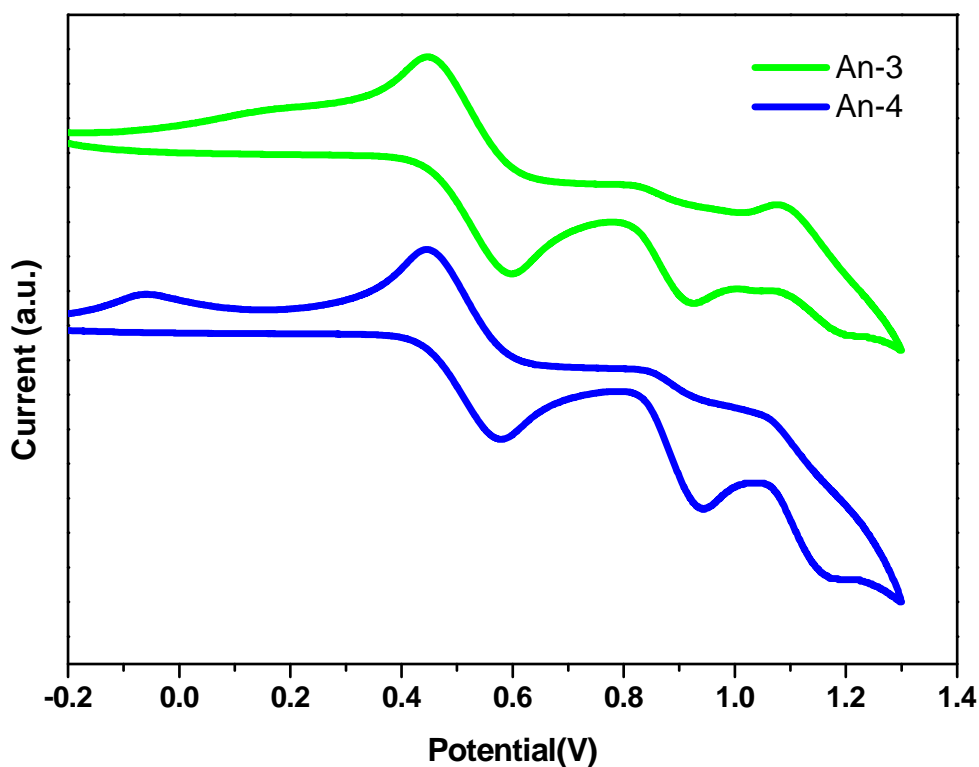
3.4. Photovoltaic Device Performances

The dye-sensitized solar cells were constructed by using these dyes as a sensitizer for nanocrystalline anatase TiO_2 particles, and the electrolyte composed of 0.05 M I_2/0.5 M LiI/0.5 M *tert*-butylpyridine in acetonitrile solution. The photovoltaic performance statistics under a solar condition (AM 1.5) illumination are collected in Table 2.

Table 2. Dye-sensitized solar cells (DSSCs) performance parameters of the dyes.

Cell	V_{OC} (V)	J_{SC} (mA/cm^2)	(%)	FF	Dye Loading (mol/cm^2)
An-1	0.62	7.10	2.85	0.65	3.97×10^{-7}
An-2	0.64	6.06	2.61	0.67	3.17×10^{-7}
An-3	0.59	7.30	2.88	0.67	2.88×10^{-7}
An-4	0.55	4.52	1.62	0.65	3.14×10^{-7}
N719	0.77	13.87	7.11	0.67	–

The photocurrent-voltage (*J-V*) curves, dark current and the incident monochromatic photo-to-current conversion efficiency (IPCE) plots of the cells were shown in Figure 5 and Figure 6, respectively. The short-circuit photocurrent density (J_{SC}), open-circuit voltage (V_{OC}) and fill factor (*FF*) of device are in the range of 4.52–7.30 mA/cm^2, 0.55–0.64 V and 0.65–0.67, respectively, corresponding to an overall conversion efficiency of 1.62%–2.88%. The reference standard of ruthenium dye N719-based cell (conversion efficiency = 7.11%) fabricated and measured under similar conditions. The cells exhibit a maximum IPCE between 450 and 500 nm and the IPCE spectra is broadened in the long wavelength side extending to 650 nm (Figure 6). The values of the dye density on TiO_2 film are also listed in Table 2 and found to decrease in the order of **An-1** (3.97×10^{-7} mol/cm^2) > **An-2** (3.17×10^{-7} mol/cm^2) > **An-4** (3.14×10^{-7} mol/cm^2) > **An-3** (2.88×10^{-7} mol/cm^2). Likely the bulkier bis-diethylfluorenyl amino group of the **An-3** results in the lowest dye density. Despite of relatively low dye density and unfavourable charge recombination with the electrolyte (vide infra), the **An-3** cell still exhibited the best performance. This outcome can be attributed to the good light harvesting efficiency (long absorption wavelength and high molar extinction coefficient) and better electron collection because of lower electron transport resistance (vide infra). In contrary, the **An-4** cell exhibited the lowest performance. This might be due to the higher dark current (Figure 5) and the inferior electron injection (vide infra). The cell efficiency of **An-1** is higher than that of **5** [34]. Apparently light harvesting plays a very important role in cell performance. The dark currents of DSSCs fabricated were also checked (Figure 5). The V_{OC} data of DSSCs decreases in the order of **N719** > **An-2** > **An-1** > **An-3** > **An-4**. Large dark currents of the cells from **An-3** and **An-4** are consistent with their lower V_{OC} values, though the influence of Fermi-level variation cannot be ruled out.

The electrochemical impedance spectroscopic (EIS) measurement under illumination was shown in Figure 7. Upon illumination of 100 mW cm^{-2} under open circuit conditions, the radius of the intermediate frequency semicircle in the Nyquist plot (Figure 7) represents the electron transport resistance. The electron transport resistance (R_{ct}) (Table 2) decreased in the order of **An-4** (107.6 Ω) > **An-2** (58.5 Ω) > **An-1** (44.0 Ω) > **An-3** (40.0 Ω) > **N719** (20.3 Ω). This is consistent with the cell performance. The aforementioned trend of dark current was also supported by the EIS

studies carried out in the dark (Figure 8). The intermediate frequency semicircle represents the charge recombination resistance on the TiO_2 surface (R_{rec}), where the larger R_{rec} value implies the smaller dark current. The R_{rec} values decreases in the order of **N719** > **An-2** > **An-1** > **An-3** > **An-4**, respectively. This is also consistent with the V_{OC} values.

Figure 5. The current density-voltage curves and dark current of DSSCs based on the dyes.
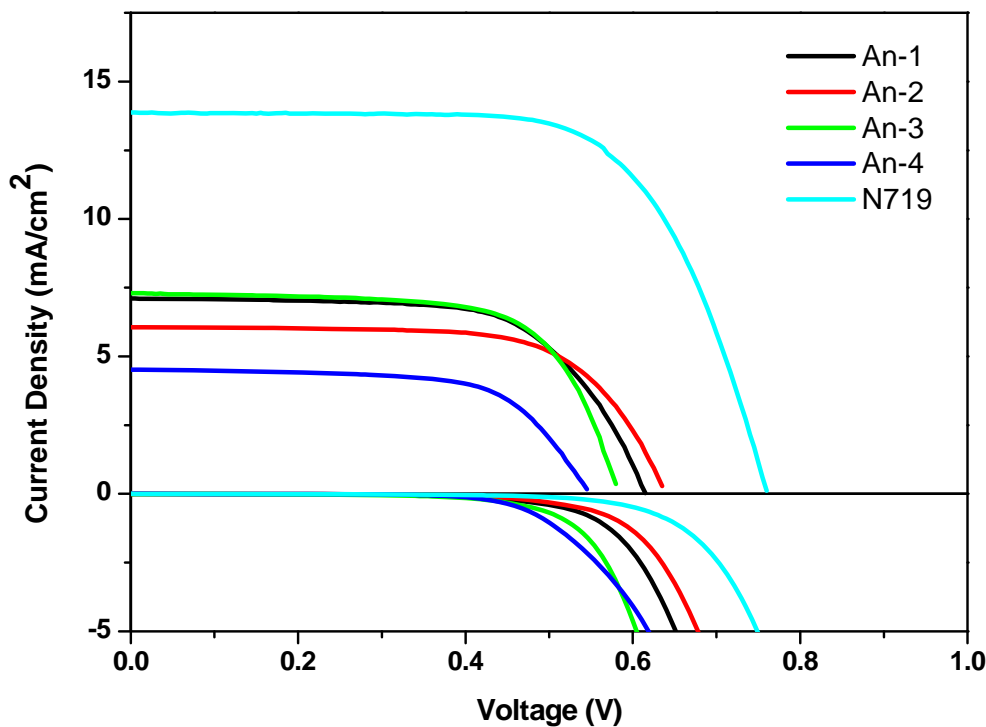
Figure 6. Incident monochromatic photo-to-current conversion efficiency (IPCE) plots for the DSSCs cells.
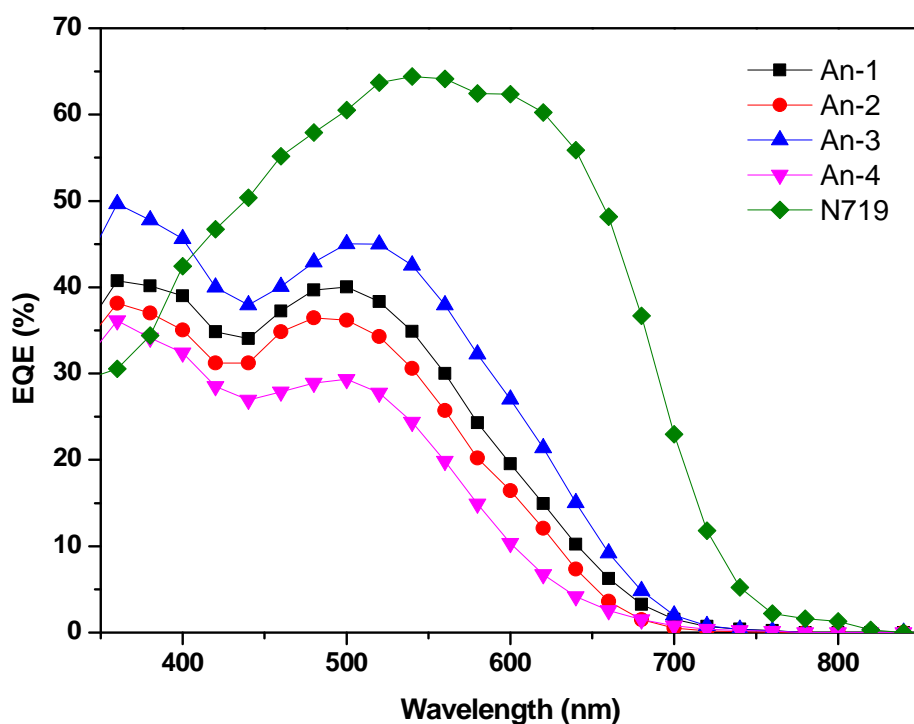
Figure 7. Electrochemical impedance spectra (Nyquist plots) of DSSC for dyes measured under illumination (AM 1.5).
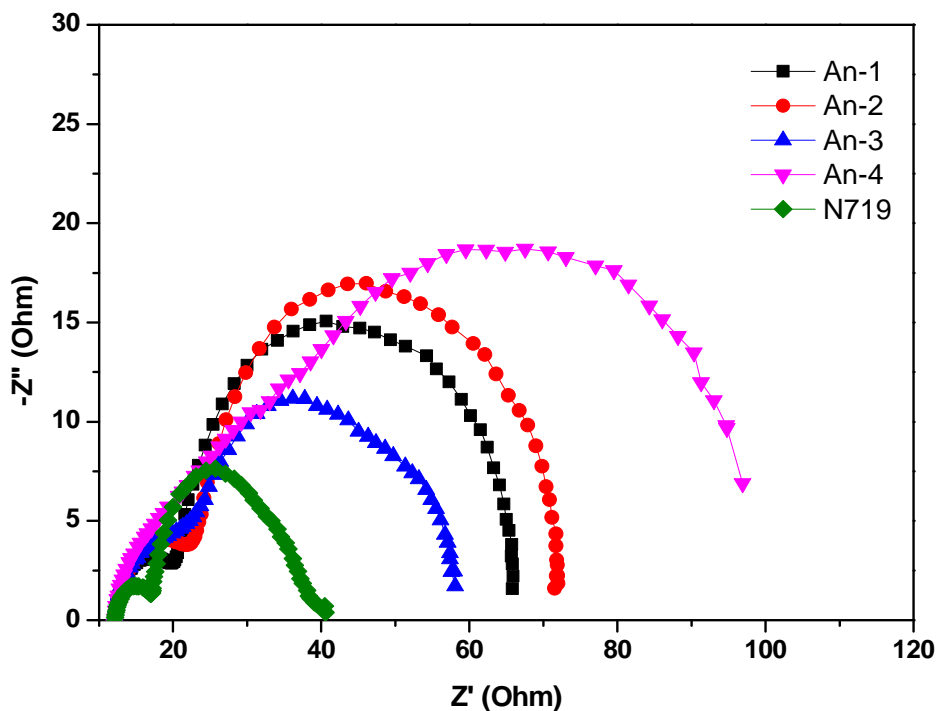
Figure 8. Electrochemical impedance spectra (Nyquist plots) of DSSC for dyes measured in the dark under −0.55 V bias.
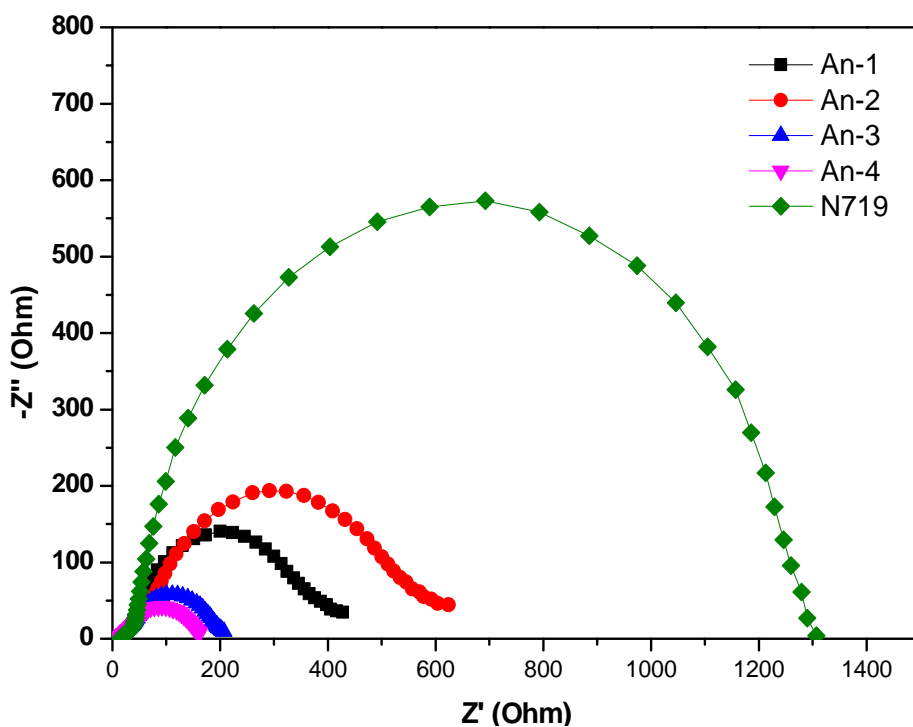
3.5. Theoretical Calculations

The series of dyes **An-1**−**An-4** have been modeled by density functional calculations at B3LYP/6-31G* level of theory. In the optimized structure, the dihedral angle between the anthracene

and the thiophene units is smaller than 23° (Figure 9), which is significantly smaller than that (37°–52°) observed in the organic sensitizers based on 1,4-naphthyl unit developed earlier by us [35]. The calculated **An-3** molecule has the highest HOMO energy level (−4.77 eV) among all, which is consistent with the electrochemical data (Figure 10).

Figure 9. Schematic division and dihedral angles of molecules.
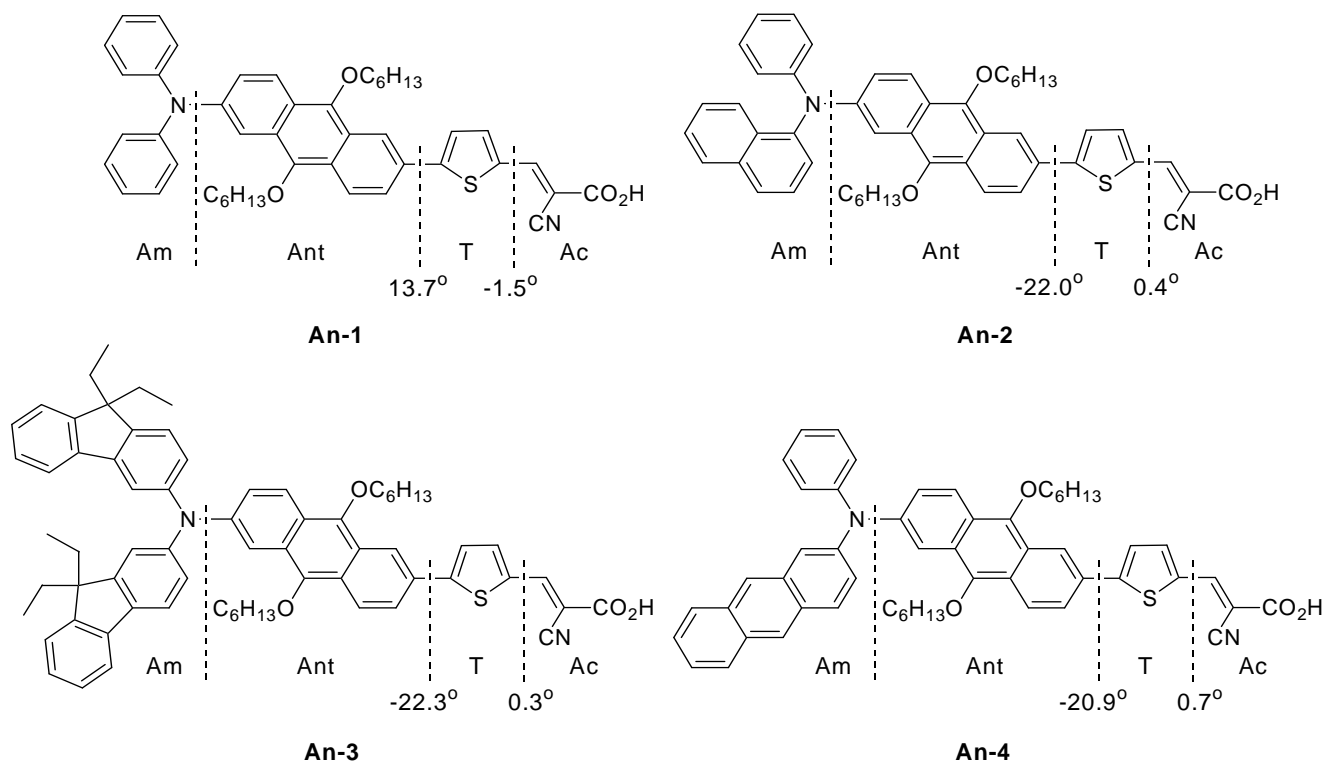
Figure 10. Schematic representation of the calculated electronic structure in the gas-phase for the dyes.
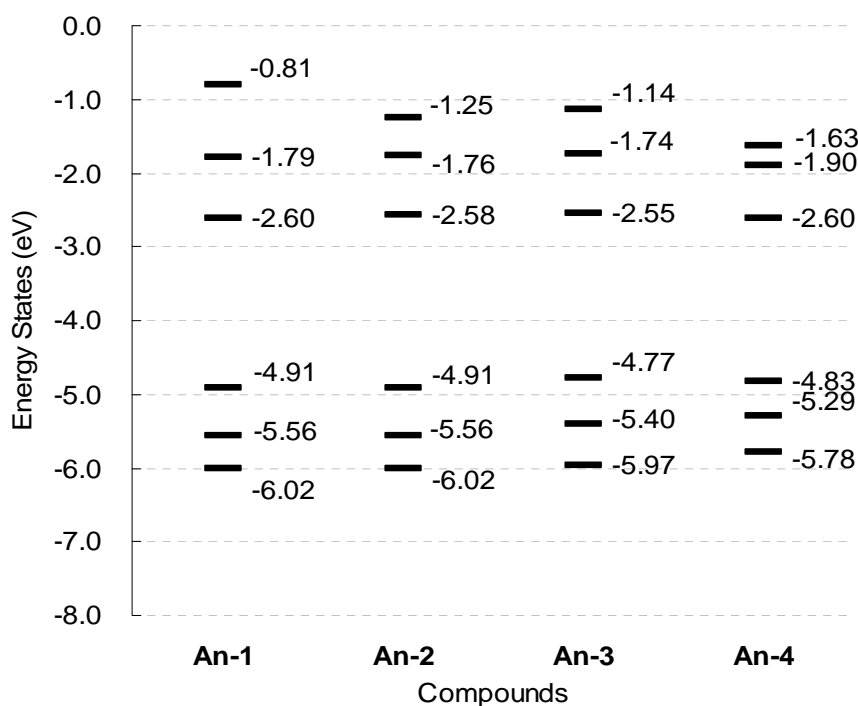
The time-dependent DFT calculations also confirm the absorption behavior of the dyes in the UV-Vis spectra (see Table 3). The $S_0 \to S_1$ excitations of the dyes having the oscillator strength between 0.55–0.60 are mainly contributed from HOMO $\to$ LUMO transitions (99%). The HOMOs of the dye largely populate on the arylamine and the anthracenyl entity, and the LUMOs are mainly populated on the thienyl entity and 2-cyanoacrylic acid (see also Figure 11). Consequently, charge transfer from both arylamine and anthracent to 2-cyanoacrylic acid is prominent. This is also supported by the analysis of Mulliken charges in different fragments (PhN/NapN/FluN/AntN: amines; Ant: 2,6-dihexyloxyanthracene; T: thiophene; Ac: 2-cyanoacrylic acid) of the dyes for the S_1 state (Figure 12).

Table 3. Calculated lower-lying transitions of the dyes.[a]

dye	State	excitation[a]	λ_{cal}, eV	f[b]	Δ(Mulliken charge),[c] $|e|$	$f \times \Delta q$
An-1	S_1	H → L (99%)	2.07	0.57	PhN: 0.28	−0.20
					Ant: 0.36	
					T: −0.29	
					Ac: −0.35	
	S_2	H2 → L (5%)	2.63	0.01	PhN: 0.36	0.00
		H1 → L (71%)			Ant: 0.18	
		H → L1 (21%)			T: −0.25	
					Ac: −0.29	
	S_3	H1 → L (89%)	2.79	0.06	PhN: 0.38	−0.01
					Ant: −0.10	
					T: −0.11	
					Ac: −0.17	
	S_4	H2 → L (90%)	3.19	1.06	PhN: 0.03	−0.13
					Ant: 0.06	
					T: 0.03	
					Ac: −0.12	
An-2	S_1	H → L (99%)	2.09	0.55	NapN: 0.25	−0.21
					Ant: 0.45	
					T: −0.31	
					Ac: −0.39	
	S_2	H1 → L (72%)	2.65	0.03	NapN: 0.40	−0.01
		H → L1 (21%)			Ant: 0.17	
					T: −0.26	
					Ac: −0.30	
	S_3	H1 → L (24%)	2.81	0.06	NapN: 0.35	−0.01
		H → L1 (74%)			Ant: −0.07	
					T: −0.11	
					Ac: −0.17	
	S_4	H → L2 (91%)	3.16	0.20	NapN: −0.49	0.00
					Ant: 0.46	
					T: 0.03	
					Ac: 0.01	

Table 3. *Cont.*

dye	State	excitation[a]	λ_{cal}, eV	f^b	Δ(Mulliken charge),[c] |e|	$f \times \Delta q$
An-3	S_1	H → L (99%)	1.99	0.60	FluN: 0.38	−0.23
					Ant: 0.32	
					T: −0.31	
					Ac: −0.39	
	S_2	H1 → L (85%)	2.55	0.00	FluN: 0.38	0.00
		H → L1 (10%)			Ant: 0.28	
					T: −0.31	
					Ac: −0.36	
	S_3	H1 → L (12%)	2.69	0.09	FluN: 0.44	−0.01
		H → L1 (85%)			Ant: −0.23	
					T: −0.08	
					Ac: −0.13	
	S_4	H2 → L (53%)	3.18	0.60	FluN: −0.03	−0.06
		H → L2 (36%)			Ant: 0.15	
					T: −0.01	
					Ac: −0.11	
An-4	S_1	H → L (99%)	1.98	0.55	AntN: 0.47	−0.21
					Ant: 0.21	
					T: −0.31	
					Ac: −0.37	
	S_2	H1 → L (95%)	2.44	0.06	AntN: 0.51	−0.02
					Ant: 0.20	
					T: −0.32	
					Ac: −0.38	
	S_3	H → L1 (93%)	2.59	0.14	AntN: 0.24	−0.01
					Ant: −0.11	
					T: −0.04	
					Ac: −0.08	
	S_4	H → L2 (92%)	2.82	0.01	AntN: −0.13	0.00
					Ant: 0.16	
					T: −0.01	
					Ac: −0.02	

[a] Results are based on gas-phase TD-DFT calculation. [b] H = HOMO, L = LUMO, H1 = The next highest occupied molecular orbital, or HOMO − 1, H2 = HOMO − 2, L1 = LUMO + 1, L2 = LUMO + 2. In parentheses is the population of a pair of MO excitations. [c] Oscillator strength. [d]The difference of the Mulliken charge between the ground state and excited state.

Figure 11. Selected frontier orbitals of the dyes.
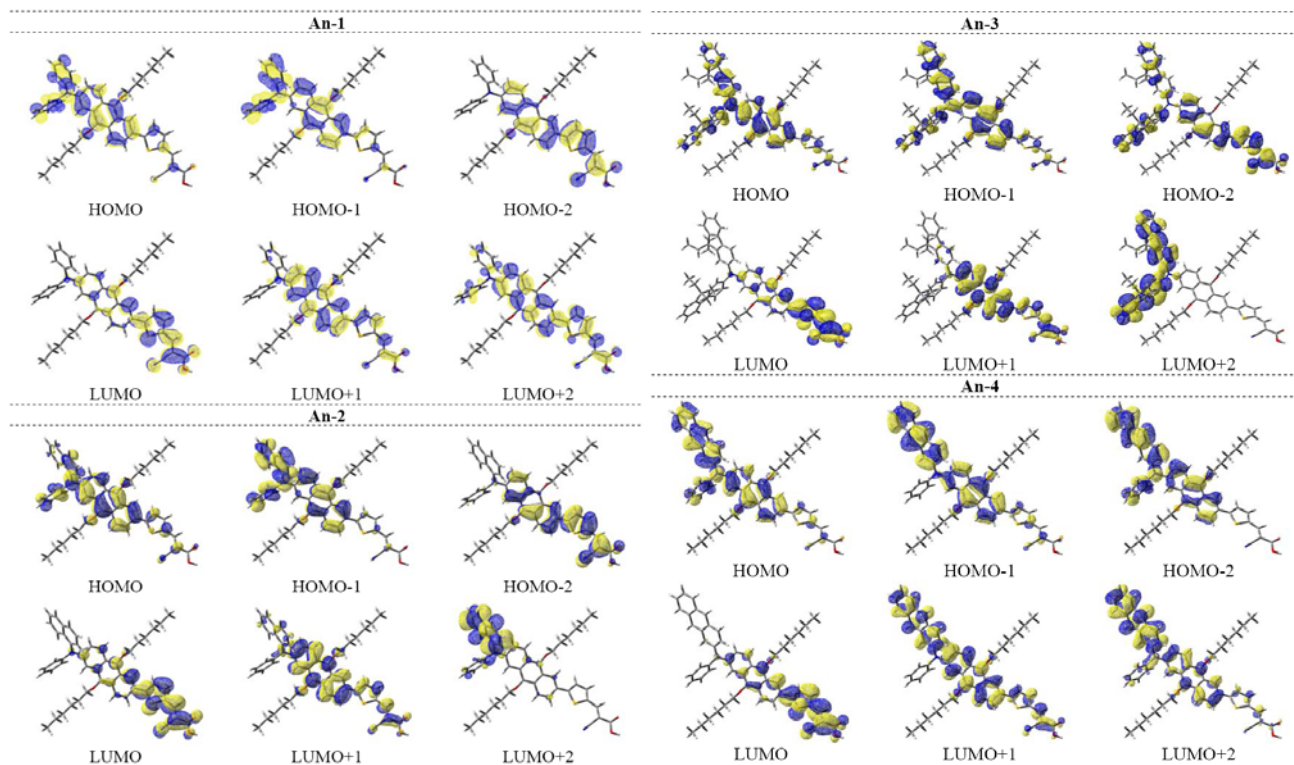
Figure 12. Plot of the difference in the Mulliken charges between the ground-state and the excited state.
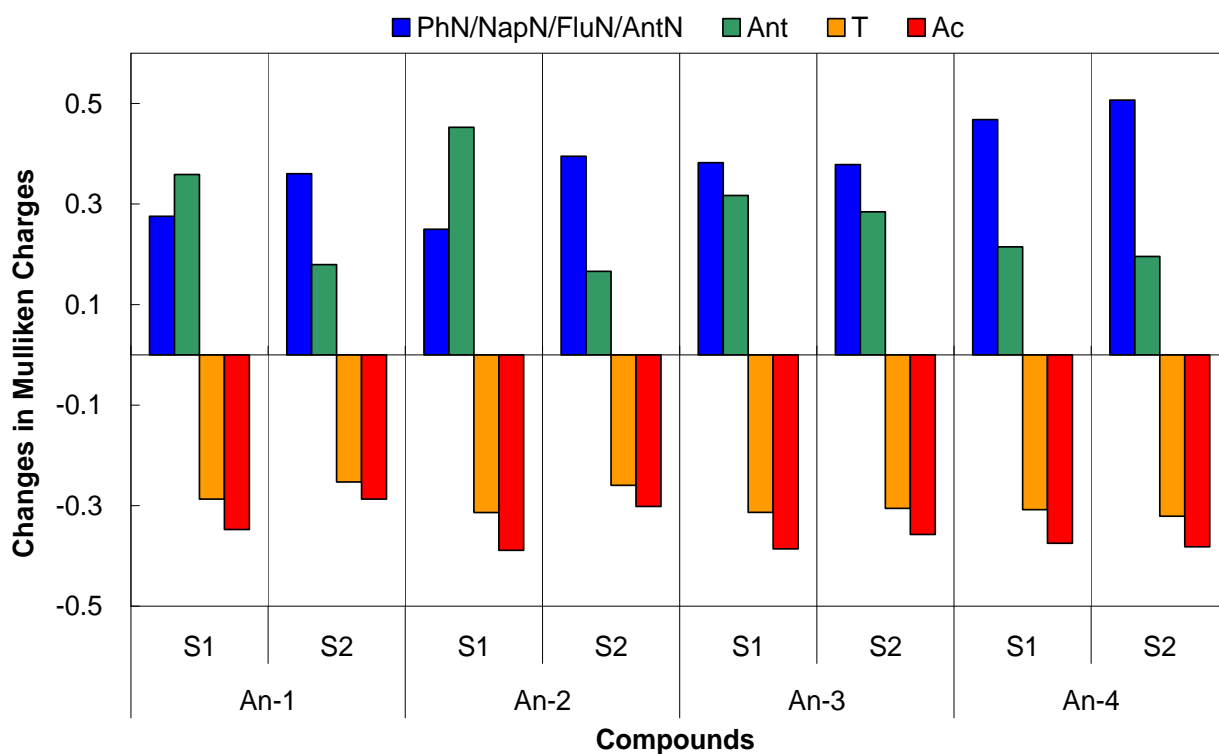
4. Conclusions

In summary, we have synthesized four novel diarylamino-based organic dyes containing a 2,6-difunctionalized anthracene entity in the conjugated spacer. The dyes have longer wavelength absorption and stronger absorption intensity than the analogous dye based on 9,10-difunctionalized anthracene bridge. DSSCs using these dyes as the sensitizers exhibited efficiencies ranging from 1.62% to 2.88% under one sun (AM 1.5) illumination. The efficiencies of DSSCs in this report also surpass that based on 9,10-difunctionalized anthracene-based sensitizer of similar structure.

Acknowledgments

References

1. O'Reagen, B.; Grätzel, M. A low-cost, high-efficiency solar cell based on dye-sensitized colloidal TiO$_2$ films. *Nature* **1991**, *353*, 737–740.
2. Grätzel, M. Recent advances in sensitized mesoscopic solar cells. *Acc. Chem. Res*. **2009**, *42*, 1788–1798.
3. Cao, Y.; Bai, Y.; Yu, Q.; Cheng, Y.; Liu, S.; Shi, D.; Gao, F.; Wang, P. Dye-sensitized solar cells with a high absorptivity ruthenium sensitizer featuring a 2-(hexylthio)thiophene conjugated bipyridine. *J. Phys. Chem. C* **2009**, *113*, 6290–6297.
4. Hagfeldt, A.; Boschloo, G.; Sun, L.C.; Kloo, L.; Pettersson, H. Dye-sensitized solar cells. *Chem. Rev*. **2010**, *110*, 6595–6663.
5. Yella, A.; Lee, H.-W.; Tsao, H.N.; Yi, C.; Chandiran, A.K.; Nazeeruddin, M.K.; Diau, E.W.-G.; Yeh, C.-Y.; Zakeeruddin, S.M.; Grätzel, M. Porphyrin-sensitized solar cells with cobalt (II/III)-based redox electrolyte exceed 12 percent efficiency. *Science* **2011**, *334*, 629–634.
6. Mishra, A.; Fischer, M.K.R.; Bauerle, P. Metal-free organic dyes for dye-sensitized solar cells: From structure: Property relationships to design rules. *Angew. Chem. Int. Ed*. **2009**, *48*, 2474–2499.
7. Chen, B.S.; Chen, D.Y.; Chen, C.L.; Hsu, C.W.; Hsu, H.C.; Wu, K.L.; Liu, S.H.; Chou, P.T.; Chi, Y. Donor-acceptor dyes with fluorine substituted phenylene spacer for dye-sensitized solar cells. *J. Mater. Chem*. **2011**, *21*, 1937–1945.
8. Zhou, D.; Cai, N.; Long, H.; Zhang, M.; Wang, Y.; Wang, P. An energetic and kinetic view on cyclopentadithiophene dye-sensitized solar cells: the influence of fluorine *vs.* ethyl substituent. *J. Phys. Chem. C* **2011**, *115*, 3163–3171.
9. Zhu, W.; Wu, Y.; Wang, S.; Li, W.; Li, X.; Chen, J.; Wang, Z.S.; Tian, H. Organic D-A-π-A solar cell sensitizers with improved stability and spectral response. *Adv. Funct. Mater*. **2011**, *21*, 756–763.
10. Ning, Z.; Fu, Y.; Tian, H. Improvement of dye-sensitized solar cells: What we know and what we need to know. *Energy Environ. Sci*. **2010**, *3*, 1170–1181.

11. Ning, Z.; Zhang, Q.; Pei, H.; Luan, J.; Lu, C.; Cui, Y.; Tian, H. Photovoltage improvement for dye-sensitized solar cells via cone-shaped structural design. *J. Phys. Chem. C* **2009**, *113*, 10307–10313.

12. Yen, Y.-S.; Chou, H.-H.; Chen, Y.-C.; Hsu, C.-Y.; Lin, J.T. Recent progress of organic materials for dye-sensitized solar cells. *J. Mater. Chem.* **2012**, *22*, 8734–8747.

13. Velusamy, M.; Justin Thomas, K.R.; Lin, J.T.; Hsu, Y.-C.; Ho, K.-C. Organic dyes incorporating low-band-gap chromophores for dye-sensitized solar cells. *Org. Lett.* **2005**, *7*, 1899–1902.

14. Justin Thomas, K.R.; Lin, J.T.; Hsu, Y.-C.; Ho, K.-C. Organic dyes containing thienylfluorene conjugation for solar cells. *Chem. Commun.* **2005**, 4098–4100.

15. Tsai, M.-S.; Hsu, Y.-C.; Lin, J.T.; Chen, H.-C.; Hsu, C.-P. Organic dyes containing 1*H*-phenanthro[9,10-*d*]imidazole conjugation for solar cells. *J. Phys. Chem. C* **2007**, *111*, 18785–18793.

16. Justin Thomas, K.R.; Hsu, Y.-C.; Lin, J.T.; Lee, K.-M.; Ho, K.-C.; Lai, C.-H.; Cheng, Y.-M.; Chou, P.-T. 2,3-Disubstituted thiophene-based organic dyes for solar cells. *Chem. Mater.* **2008**, *20*, 1830–1840.

17. Yen, Y.-S.; Hsu, Y.-C.; Lin, J.T.; Chang, C.-W.; Hsu, C.-P.; Yin, D.-J. Pyrrole-based organic dyes for dye-sensitized solar cells. *J. Phys. Chem. C* **2008**, *112*, 12557–12567.

18. Huang, S.-T.; Hsu, Y.-C.; Yen, Y.-S.; Chou, H.-H.; Lin, J.T.; Chang, C.-W.; Hsu, C.-P.; Tsai, C.; Yin, D.-J. Organic dyes containing a cyanovinyl entity in the spacer for solar cells applications. *J. Phys. Chem. C* **2008**, *112*, 19739–19747.

19. Lin, J.T.; Chen, P.-C.; Yen, Y.-S.; Hsu, Y.-C.; Chou, H.-H.; Yeh, M.-C.P. Organic dyes containing furan moiety for high-performance dye-sensitized solar cells. *Org. Lett.* **2009**, *11*, 97–100.

20. Velusamy, M.; Hsu, Y.-C.; Lin, J.T.; Chang, C.-W.; Hsu, C.-P. 1-Alkyl-1*H*-imidazole-based dipolar organic compounds for dye-sensitized solar cells. *Chem. Asian J.* **2010**, *5*, 87–96.

21. Chen, C.-H.; Hsu, Y.-C.; Chou, H.-H.; Justin Thomas, K.R.; Lin, J.T.; Hsu, C.-P. Dipolar compounds containing fluorene and a heteroaromatic ring as the conjugating bridge for high-performance dye-sensitized solar cells. *Chem. Eur. J.* **2010**, *16*, 3184–3193.

22. Silvestri, V.; Marrocchi, A.; Seri, M.; Kim, C.; Mark, T.J.; Facchetti, A.; Taticchi, A. Solution-processable low-molecular weight extended arylacetylenes: versatile p-type semiconductors for field-effect transistors and bulk heterojunction solar cells. *J. Am. Chem. Soc.* **2010**, *132*, 6108–6123.

23. Chung, D.S.; Park, J.W.; Park, J.H.; Moon, D.; Kim, G.H.; Lee, D.H.; Shim, H.K.; Kwon, S.K.; Park, C.E. High mobility organic single crystal transistors based on soluble triisopropylsilylethynyl anthracene derivatives. *J. Mater. Chem.* **2010**, *20*, 524–530.

24. Jung, K.H.; Bae, S.Y.; Kim, K.H.; Cho, M.J.; Lee, K.; Kim, Z.H.; Choi, D.H.; Chung, D.S.; Park, C.E. High-mobility anthracene-based X-shaped conjugated molecules for thin film transistors. *Chem. Commun.* **2009**, 5290–5292.

25. Xia, Z.Y.; Zhang, Z.Y.; Su, J.H.; Zhang, Q.; Fung, K.M.; Lam, M.K.; Li, K.F.; Wong, W.Y.; Cheah, K.W.; Tian, H.; Chen, C.H. Robust and highly efficient blue light-emitting hosts based on indene-substituted anthracene. *J. Mater. Chem.* **2010**, *20*, 3768–3774.

26. Reddy, M.A.; Thomas, A.; Srinivas, K.; Rao, V.J.; Bhanuprakash, K.; Sridhar, B.; Kumar, A.; Kamalasanan, M.N.; Srivastava, R. Synthesis and characterization of 9,10-bis(2-phenyl-1,3,4-oxadiazole) derivatives of anthracene: Efficient n-type emitter for organic light-emitting diodes. *J. Mater. Chem.* **2009**, *19*, 6172–6184.

27. Tao, S.; Zhou, Y.; Lee, C.S.; Lee, S.T.; Huang, D.; Zhang, X. Highly efficient nondoped blue organic light-emitting diodes based on anthracene-triphenylamine derivatives. *J. Phys. Chem. C* **2008**, *112*, 14603–14606.

28. Wang, L.; Wong, W.-Y.; Lin, M.-F.; Wong, W.-K.; Cheah, K.-W.; Tam, H.-L.; Chen, C.H. Novel host materials for single-component white organic light-emitting diodes based on 9-naphthylanthracene derivatives. *J. Mater. Chem.* **2008**, *18*, 4529–4536.

29. Xia, Z.-Y.; Su, J.-H.; Wong, W.-Y.; Wang, L.; Cheah, K.-W.; Tian, H.; Chen, C.H. High performance organic light-emitting diodes based on tetra(methoxy)-containing anthracene derivatives as a hole transport and electron-blocking layer. *J. Mater. Chem.* **2010**, *20*, 8382–8388.

30. Wang, L.; Wu, Z.-Y.; Wong, W.-Y.; Cheah, K.-W.; Huang, H.; Chen, C.H. New blue host materials based on anthracene-containing dibenzothiophene. *Org. Electron.* **2011**, *12*, 595–601.

31. Marrocchi, A.; Silvestri, F.; Seri, M.; Facchetti, A.; Taticchi, A.; Marks, T.J. Conjugated anthracene derivatives as donor materials for bulk heterojunction solar cells: Olefinic *versus* acetylenic spacers. *Chem. Commun.* **2009**, 1380–1382.

32. Teng, C.; Yang, X.; Yang, C.; Li, S.; Cheng, M.; Hagfeldt, A.; Sun, L. Molecular design of anthracene-bridged metal-free organic dyes for efficient dye-sensitized solar cells. *J. Phys. Chem. C* **2010**, *114*, 9101–9110.

33. Srinivas, K.; Yesudas, K.; Bhanuprakash, K.; Rao, V.J.; Giribabu, L. A combined experimental and computational investigation of anthracene based sensitizers for DSSC: comparison of cyanoacrylic and malonic acid electron withdrawing groups binding onto the TiO_2 anatase (101) surface. *J. Phys. Chem. C* **2009**, *113*, 20117–20126.

34. Thomas, K.R.J.; Singh, P.; Baheti, A.; Hsu, Y.-C.; Ho, K.-C.; Lin, J.T. Electro-optical properties of new anthracene based organic dyes for dye-sensitized solar cells. *Dye. Pigment.* **2011**, *91*, 33–43.

35. Chen, Y.-C.; Chen, Y.-H.; Chou, H.-H.; Chaurasia, S.; Wen, Y.S.; Lin, J.T.; Yao, C.-F. Naphthyl and thienyl units as bridges for metal-free dye-sensitized solar cells. *Chem. Asian J.* **2012**, *7*, 1074–1084.

36. *Q-CHEM*, version 4.0; Q-Chem Inc.: Pittsburgh, PA, USA, 2011.

37. Vaswani, H.M.; Hsu, C.P.; Head-Gordon, M.; Fleming, G.R. Quantum chemical evidence for an intramolecular charge-transfer state in the carotenoid peridinin of peridinin−chlorophyll−protein. *J. Phys. Chem. B* **2003**, *107*, 7940–7946.

38. Kurashige, Y.; Nakajima, T.; Kurashige, S.; Hirao, K.; Nishikitani, Y. Theoretical investigation of the excited states of coumarin dyes for dye-sensitized solar cells. *J. Phys. Chem. A* **2007**, *111*, 5544–5548.

39. Dreuw, A.; Head-Gordon, M. Failure of time-dependent density functional theory for long-range charge-transfer excited states: The zincbacteriochlorin–bacteriochlorin and bacteriochlorophyll–spheroidene complexes. *J. Am. Chem. Soc.* **2004**, *126*, 4007–4016.

40. Tamao, K.; Sumitani, K.; Kumada, M. Selective carbon-carbon bond formation by cross-coupling of Grignard reagents with organic halides. Catalysis by nickel-phosphine complexes. *J. Am. Chem. Soc.* **1972**, *94*, 4374–4376.

41. Hartwig, J.F.; Kawatsura, M.; Hauck, S.I.; Shaughnessy, L.M.; Alcazar-Roman, J. Room-temperature palladium-catalyzed amination of aryl bromides and chlorides and extended scope of aromatic C−N bond formation with a commercial ligand. *J. Org. Chem.* **1999**, *64*, 5575–5580.

42. Driver, M.S.; Hartwig, J.F. A second-generation catalyst for aryl halide amination: Mixed secondary amines from aryl halides and primary amines catalyzed by (DPPF)PdCl$_2$. *J. Am. Chem. Soc.* **1996**, *118*, 7217–7218.

43. Kim, S.; Choi, H.; Baik, C.; Song, K.; Kang, S.O.; Ko, J. Novel conjugated organic dyes containing bis-dimethylfluorenyl amino phenyl thiophene for efficient solar cell. *Tetrahedron* **2007**, *63*, 11436–11443.

44. Hara, K.; Sato, T.; Katoh, R.; Furube, A.; Ohga, Y.; Shinpo, A.; Suga, S.; Sayama, K.; Sugihara, H.; Arakawa, H. Molecular design of coumarin dyes for efficient dye-sensitized solar cells. *J. Phys. Chem. B* **2003**, *107*, 597–606.

45. Hara, K.; Tchibana, Y.; Ohga, Y.; Shinpo, A.; Suga, S.; Sayama, K.; Sugihara, H.; Arakawa, H. Dye-sensitized nanocrystalline TiO$_2$ solar cells based on novel coumarin dyes. *Sol. Energy Mater. Sol. Cells* **2003**, *77*, 89–103.

46. Li, S.-L.; Jiang, K.-J.; Shao, K.-F.; Yang, L.-M. Novel organic dyes for efficient dye-sensitized solar cells. *Chem. Commun.* **2006**, 2792–2794.

47. Hagfeldt, A.; Grätzel, M. Light-induced redox reactions in nanocrystalline systems. *Chem. Rev.* **1995**, *95*, 49–68.